arXiv:0905.2654v1 [astro-ph.GA] 16 May 2009

The variability of Sagittarius A* at 3 millimeter

Juan Li[1,2], Zhi-Qiang Shen[1], Atsushi Miyazaki[3], Lei Huang[4], R. J. Sault[5], Makoto Miyoshi[3], Masato Tsuboi[6] and Takahiro Tsutsumi[3]

ABSTRACT

We have performed monitoring observations of the 3-mm flux density toward the Galactic Center compact radio source Sgr A* with the Australia Telescope Compact Array since 2005 October. Careful calibrations of both elevation-dependent and time-dependent gains have enabled us to establish the variability behavior of Sgr A*. Sgr A* appeared to undergo a high and stable state in 2006 June session, and a low and variable state in 2006 August session. We report the results, with emphasis on two detected intra-day variation events during its low states. One is on 2006 August 12 when Sgr A* exhibited a 33% fractional variation in about 2.5 hr. The other is on 2006 August 13 when two peaks separated by about 4 hr, with a maximum variation of 21% within 2 hr, were seen. The observed short timescale variations are discussed in light of two possible scenarios, i.e., the expanding plasmon model and the sub-Keplerian orbiting hot spot model. The fitting results indicate that for the adiabatically expanding plasmon model, the synchrotron cooling can not be ignored, and a minimum mass-loss rate of $9.7 \times 10^{-10} M_{\odot}$ yr^{-1} is obtained based on parameters derived for this modified expanding plasmon model. Simultaneous multi-wavelength observation is crucial to our understanding the physical origin of rapid radio variability in Sgr A*.

Subject headings: Galaxy: center, techniques: interferometric

[1]Key Laboratory for Research in Galaxies and Cosmology, Shanghai Astronomical Observatory, Chinese Academy of Sciences, 80 Nandan RD, Shanghai 200030, China; lijuan@shao.ac.cn, zshen@shao.ac.cn

[2]Graduate School of the Chinese Academy of Sciences, Beijing 100039, China

[3]National Astronomical Observatory of Japan, 2-21-1 Osawa, Mitaka, Tokyo 181-8588, Japan; amiya@miz.nao.ac.jp, makoto.miyoshi@nao.ac.jp, t.tsutsumi@nao.ac.jp

[4]Key Laboratory for Research in Galaxies and Cosmology, University of Science and Technology of China, Hefei 230026, China; mlhuang@ustc.edu.cn

[5]University of Melbourne, School of Physics, Parkville, Victoria 3052, Australia; rsault@unimelb.edu.au

[6]Institute of Space and Astronautical Science, Sagamihara, Kanagawa 229-8510, Japan; tsuboi@vsop.isas.jaxa.jp

1. Introduction

There is compelling evidence that Sagittarius A* (Sgr A*), the extremely compact radio source at the dynamical center of the Galaxy, is associated with a $4 \times 10^6 M_\odot$ black hole (Eckart & Genzel 1996; Ghez et al. 2000; Schödel et al. 2002; Eisenhauer 2003). Since its discovery in 1974 (Balick & Brown 1974), Sgr A* has been observed extensively with radio telescopes in the northern hemisphere, and temporal flux variations at millimeter wavelengths were reported. With VLA observations, Yusef-Zadeh et al. (2006b) detected an increase of flux density at a fractional level of 7% and 4.5% at 7- and 13-mm, respectively, with a duration of about 2 hr. The peak flare emission at 7-mm led the 13-mm peak flare by 20-40 minutes. Mauerhan et al. (2005) detected intra-day variations (IDVs) of about 20% and in some cases up to 40% at 3-mm using the Owens Valley Radio Observatory (OVRO). The rise and decay occurred on a timescale of 1-2 hr. At 2-mm, Miyazaki et al. (2004) reported a 30% flux increase in 30 minutes from the monitoring of the Nobeyama Millimeter Array (NMA). On the other hand, flares with violent intensity increases in very short timescales have also been detected at infrared and X-ray bands (Genzel et al. 2003; Baganoff et al. 2001; Eckart et al. 2006b), inferring that these emissions from Sgr A* originate within very vicinity of the central massive black hole. This is further strengthened by the simultaneous detection of X-ray, infrared and sub-mm flares (Eckart et al. 2004, 2006a, 2008a, 2008b; Yusef-Zadeh et al. 2006a, 2008; Marrone et al. 2008).

Since Sgr A* is embedded in thick thermal material, it is particularly difficult to observe its intrinsic structure. But observations of IDV can give indirect constraints on the source emission geometry and emission mechanisms. However, previous monitoring observations of Sgr A* from the northern hemisphere have been strictly limited to a short observing window (< 7 hr/day) for the Galactic Center region. We have performed monitoring observations of flux density toward Sgr A* at 3-mm since 2005 October when for the first time the Australia Telescope Compact Array (ATCA) of the Australia Telescope National Facility (ATNF) was available at 3-mm. The ATCA is an interferometer consisting of five 22-m radio telescopes at Narrabri, Australia where Sgr A* passes almost overhead, allowing a much longer observing window (> 8 hr at elevation angles above 40°). As such, the ATCA calibrations and flux density measurements of Sgr A* are expected to be more accurate.

In this paper, we report our effort to search for IDV in Sgr A* with the ATCA. We first introduce the ATCA observations in § 2. The data reduction and analysis with emphasis on the gain calibrations are described in detail in § 3. In § 4, we present the detection of IDV events in Sgr A*. To interpret the observation, we discuss two possible scenarios in § 5, followed by a summary in § 6. Throughout this paper, the fractional variation is defined as

$\frac{S_{max}-S_{min}}{\frac{1}{2}(S_{max}+S_{min})}$, here S_{max} and S_{min} refer to the maximum and minimum value of flux density, respectively.

2. OBSERVATIONS

In 2005 and 2006, we performed 3-mm ATCA flux density monitoring of Sgr A* over 50 hr in the following 3 sessions: 2005 October 18, 2006 June 9 and August 9-13. Dual (linear) polarization double sideband (DSB) HEMT receivers were used. The first ever 3-mm ATCA monitoring of Sgr A* was performed on 2005 October 18 when the data were simultaneously recorded, in both the lower (93.504 GHz) and upper (95.552 GHz) sidebands, in 32 channels of a total bandwidth of 128 MHz. For the observations in 2006, the data were recorded in two slightly different 3-mm bands: the lower sideband (86.243 GHz) was set to the transition frequency of the SiO J=2-1 v=1 line with 256 channels of a total bandwidth of 16 MHz, the upper sideband (88.896 GHz) was a wideband with 32 channels of a total bandwidth of 128 MHz. Since the continuum data of the lower sideband with narrow bandwidth have relatively low signal to noise ratio, only the upper sideband data were used for Sgr A* and other continuum sources.

On 2005 October 18, we observed Sgr A* in the H168C configuration of the ATCA, with a maximum baseline of 192 m, uv range of 13 - 61kλ and a synthesized beam of $2.''9\times1.''7$. On 2006 June 9, the observations were performed in the 1.5D configuration with a maximum baseline of 1439 m, covering uv range of 20 - 430kλ and yielding a synthesized beam of $2.''1 \times 0.''3$. In 2006 August, the observations were performed in SPLIT5 configuration with a maximum baseline of 1929 m, covering uv range of 3 - 570kλ and yielding a synthesized beam of $1.''3 \times 0.''2$. In this array, the spacing between antennas 2 and 3 and antennas 3 and 4 are only 31 m, causing severe shadow effect, especially for antenna 3.

Quasar 3C 279 was observed for 10 minutes at the beginning of the observation to calibrate bandpass. Either a planet or a bright radio source was observed for the flux density calibration. The first 3-mm ATCA observation of Sgr A* lasted for 10 hr on 2005 October 18. It alternated between Sgr A* and the only secondary calibrator PKS 1730-130, which was also used as pointing calibrator. The primary calibrator Uranus was observed for 10 minutes at the end of the observation. In 2006 June and August, we observed Sgr A* in a total of 6 days with a thoughtful calibration strategy. Up to four secondary calibrators (control sources) including an SiO maser source (OH2.6-0.4) and three continuum sources (PKS 1921-293, PKS 1710-269 and PKS 1730-130) were observed to check the consistency of the gain calibrations. Limited by the weather, ATCA observed Sgr A* for only 1 hr on August 9, 4 hr on August 10 and 2 hr on August 11. Therefore, we will focus on the

measurements on June 9, August 12 and 13. The pointing accuracy was checked every half an hour by observing VX Sgr, a known strong SiO maser source. The instrumental gain and phase were calibrated by alternating observations of Sgr A* and all secondary calibrators. In 2006 June, the observations were performed using the following sequence: OH2.6-0.4 (2 min), Sgr A* (5 min), PKS 1730-130 (2 min), and PKS 1921-293 (1 min). In 2006 August, the observing sequence was PKS 1710-269 (2 min), OH2.6-0.4 (1 min), Sgr A* (10 min), PKS 1710-269 (2 min), OH2.6-0.4 (1 min), PKS 1730-130 (1 min), and PKS 1921-293 (1 min). The observing details have been summarized in Table 1.

3. DATA REDUCTION AND ANALYSIS

All the data processing was conducted using the ATNF MIRIAD package (Sault et al. 1995). At millimeter wavelengths, the atmosphere can no longer be approximately transparent. The opacity effect is included in an effective system temperature - the so-called "above atmosphere" system temperature (Ulich 1980) for the ATCA measurements at 3-mm. The bandpass corrections were made using the strong ATCA calibrator 3C279. For amplitude calibration, we first applied a nominal elevation-dependent gains of the antennas and then used calibrators to further determine the additional corrections. On 2005 October 18, the flux scale was based on observation of Uranus. On 2006 June 9, the flux density scale was determined using PKS 1730-130, assuming its flux density of 2.27 Jy at 3-mm. In 2006 August, we derived the flux density scale with another brighter radio source PKS 1921-293, which is reported to be 8.44 Jy during our observations from the ATCA calibrator list on web. From the ATCA calibrator flux density monitoring data during 2003 to 2006, we estimated its mean flux density of 8.66 Jy with a standard deviation of 1.04, implying a dispersion of about 12%. PKS 1921-293 is probably better than that of other calibrators simply because PKS 1921-293 data usually have very high signal-to-noise ratio. So, we expect an accuracy $\leq 20\%$ for the absolute amplitude calibration in these observations. After the phase self-calibration, the data were averaged in 5 minutes bin to search for shorter timescale variability. The flux density of Sgr A* was estimated by fitting a point source model to visibilities on the projected baselines longer than 25kλ (about 85 m at 3-mm) to suppress the contamination from the surrounding extended components (Miyazaki et al. 2004; Mauerhan et al. 2005). Both the fitting error reported by MIRIAD and the rms of the residual visibilities were used to get the final error estimate.

In order to establish strong cases for variability of Sgr A* at millimeter wavelengths, reliable calibrations of both elevation- and time-dependent gains are crucial. We have carefully considered and corrected the following factors that could affect the measurements during the

calibration process.

1. Antenna gain varies with elevation angle mainly because of the gravitational distortion of the dish. The antenna efficiency of ATCA has maximum value at an elevation angle of 60° and minimum value at an elevation angle of 90°. A nominal gain-elevation correction in MIRIAD is applied at elevations greater than 40° for 3-mm observations, only those data observed at elevation angles above 40° were used. However, such nominal elevation-dependent gains built in MIRIAD seem hard to fully compensate the gain variation. We have plotted flux density as a function of elevation angle and found that a nearby calibrator was needed to make further correction, otherwise significant elevation effect (e.g., peaks at about 60°, or reaches the lowest point at 90° elevation angle) will be shown up in the light-curve, which often indicates some calibration errors. PKS 1730-130, which is often used to calibrate phase and amplitude during observations from northern hemisphere at mm wavelength (e.g. Miyazaki et al. 2004, Yusef-Zadeh et al. 2008), is proved to be unsuitable for the ATCA observations. It is 16.2° away from Sgr A*, and its elevation angle is only 72° when Sgr A* reaches the zenith. Thus, gain corrections derived from this source data cannot fully compensate the elevation effect in Sgr A*, especially for observations at high elevations. Similarly, PKS 1921-293, which reaches the zenith 2 hr later than Sgr A*, is not suitable, either. So we only use two closer sources PKS 1741-312 and OH2.6-0.4 for the gain calibration.

2. Calibrators are, in general, variable sources which will unavoidably introduce uncertainties into the nominal time-independent gains. For this reason, several secondary calibrators were actually scheduled to check the consistency. The complex gains derived from one control source were applied to both Sgr A* and other control sources. If such a control source is strongly variable, a somehow similar trend in light-curve will appear for all the other sources (including Sgr A*) after calibration.

To check the significance of any detected variability, we introduced the modulation index, which is defined as the rms of the gain correction of five antennas derived from calibrators and flux density of Sgr A* divided by their mean, corresponding to the degree of variation for Sgr A*, and the fractional uncertainty in time-dependent gain correction, respectively. Obviously, if the modulation index of Sgr A* flux density is much larger than that of antenna gain correction, the detected flux variation is most likely to be real. The modulation indices of Sgr A* and gain correction of five antennas derived from two nearby calibrators OH2.6-0.4 and PKS 1710-269 on 2006 June 9, August 12 and 13 are plotted in Figure 1. The modulation indices of Sgr A* were quite large on 2006 August 12 and 13, indicating the real detection of IDV from Sgr A*. As mentioned in § 2, many data obtained from antenna 3 in 2006 August were shadowed and thus not used in obtaining its gain correction, resulting

in a large fluctuation in its gain correction and thus a bigger modulation index. During observations in 2006 August, the 3-mm flux density of PKS 1710-269 is around 0.5 Jy, only one fiftieth of that of OH2.6-0.4, therefore the signal-to-noise ratio of PKS 1710-269 data is much lower than that of OH2.6-0.4. This explains why the modulation indices of gain corrections derived from PKS 1710-269 are relatively high.

3. As mentioned in § 2, we only used upper sideband (88.896 GHz) data with a bandwidth of 128 MHz for Sgr A* and other continuum control sources, and the lower sideband (86.243 GHz) data of 32 MHz bandwidth only for the SiO maser source OH2.6-0.4. Will there be an additional uncertainty when applying to Sgr A* the gain solutions derived from OH2.6-0.4 data? We inspect this by comparing the results of the two sidebands on 2006 August 12 and 13. Similar to what we did for the upper sideband data, the flux densities of Sgr A* was also estimated from the lower sideband using the same channels as OH2.6-0.4. The results from the lower sideband data show larger error bars mainly because of the relatively low signal-to-noise ratio. The average deviations from results of upper sideband data are 2.4% on August 12 and 3.6% on August 13, much smaller than the fractional variation of Sgr A* (see § 4).

4. We also consider the response of feeds to polarized emission. The feed of ATCA is linearly polarized, and its response to a signal is a combination of total and linear polarized intensity. Thus, two polarization products, XX and YY correlations can be used as a direct measure of total intensity only when a calibrator is not linearly polarized. Unfortunately, polarizations of nearly 27% were observed in OH2.6-0.4 (Glenn et al. 2003). In addition, for ATCA antennas on altazimuth mounts, their feeds rotate with respect to the equatorial frame. This causes the actual response of ideal linearly polarized feeds to vary with the parallactic angle. To solve this problem, we used total intensity by summing the two polarization products (XX and YY) to remove the effect of linear polarization of the SiO maser OH2.6-0.4, and then derived the gain correction. In other words, a single joint solution was determined. This is generally a reasonable approximation given that antenna gains are dominated by changes common to both polarizations and, the difference between them is only a few percent and can be ignored safely (Maxim Voronkov, private communication).

Overall, OH2.6-0.4, which is relatively stable and close to Sgr A* (about 2.7° away), proved to be the best control source. As such, it was used as the main secondary calibrator to determine the antenna gain corrections for all the results presented in this paper.

4. RESULTS

During the first 3-mm ATCA observation of Sgr A* on 2005 October 18, the flux density of Sgr A* ran up to 3.5 Jy, much brighter than the normally expected 1.5 Jy in the quiescent phase, and thus Sgr A* was very likely to be in an active phase during our observation. Although Sgr A* seems to vary in its total flux density as a function of time, we can not rule out the possibility of the elevation-dependent gain effect as use of the only secondary calibrator PKS 1730-130 (16.2° from Sgr A*) severely limited the amplitude calibration. Because of this, starting from observations in 2006 June and August (see § 2), we paid a particular attention to the strategy of calibration. As a result, the light-curves of Sgr A* at 3-mm in 2006 are reliably obtained (Figure 2). All the data were calibrated using OH2.6-0.4. The flux densities were estimated by fitting a point source model to visibility data on the projected baselines longer than 25kλ. Following is a detailed description of the results from each observation.

The flux density of Sgr A* was relatively high (around 3 Jy) but stable on 2006 June 9. As shown in Figure 1, the modulation index of Sgr A* is small and comparable to that of antenna gains. Therefore, no IDV was detected.

During the first three days in the 2006 August session (August 9, 10 and 11), very limited data were available. The flux density of Sgr A* was decreased from 2.52 to 2.25 Jy in 1 hr on August 9, stayed around 1.9 Jy quite stably during the 4 hr run on August 10 and around 2.0 Jy over the 2 hr observation on August 11. So, we conclude that no ascertained IDV was detected.

Two clear IDV events were seen in the last two days of the 2006 August session. As shown in the light-curves of Sgr A* and other sources on 2006 August 12 (Figure 3 left), first the flux density of Sgr A* decreased from 1.65 to 1.50 Jy, and then increased to 2.11 Jy in 2.5 hr before decreasing again to 1.90 Jy. The fractional flux density variation is estimated to be 33%. On 2006 August 13 (Figure 3 right), the flux density of Sgr A* first increased from 1.95 to 2.14 Jy, reached its first peak before decreasing to 1.80 Jy in 1.7 hr. Then it reached the second peak 2.22 Jy in 1.9 hr, and declined to 1.98 Jy in 1.2 hr. The maximum fractional flux density variation is 21% with a timescale of about 2 hr. As shown in Figure 1, the modulation indices of Sgr A* on both August 12 and 13 are much greater than that of gain corrections, supporting that the observed flux density variations are most likely to be real.

The NMA observations of Sgr A* from 1996 to 2003 indicate that Sgr A* has quiescent and active phases, the peaks of flares were 2-3 Jy at 3-mm while the mean flux density in a quiescent phase was 1.1 $\pm$ 0.2 Jy at 90 GHz (Tsutsumi et al. 2002, Miyazaki et

al. 2003), which are in accord with our ATCA observations. As is shown in Figure 2, the mean flux density of Sgr A* dropped from 2.97 to 2.16 Jy from 2006 June to August session. The day-to-day fractional variation of Sgr A* appeared to be low from 2006 August 10 to 13. Comparison of flux densities in two observing sessions in 2006 indicates that Sgr A* appeared to undergo a high state in 2006 June session, and a low state in 2006 August session. Such different states were also noted by Herrnstein et al. (2004). They found a bimodal distribution of flux densities at centimeter wavelength and thought that it might indicate the existence of two distinct states of accretion onto the supermassive black hole. Different radiation states usually have connections to certain physical parameters or radiation model. For example, a unified inner advection dominated accretion flow (ADAF) model with different accretion rates and consequently different geometries of accretion flow has been proposed to explain five distinct spectral states that have been identified in black hole X-ray binaries (BHXBs), namely the quiescent, low, intermediate, high and very high states (Esin et al. 1997). Supposing that the accretion model of Sgr A* has something in common with that of BHXBs, the accretion rate in 2006 August session should be smaller than that in June session, but the accretion rate may not change much over days in August.

5. DISCUSSIONS

Several models have been invoked to explain the flaring activity of Sgr A*, such as the expanding plasmon model and orbiting hot spot model. We will discuss them separately.

5.1. The Plasmon Model

Expanding plasmon model of van der Laan (1966) was invoked to explain observed time delay in variation of Sgr A* at 7- and 13-mm (Yusef-Zadeh et al. 2006a, 2006b, 2008). In this model, rather than the synchrotron cooling, the adiabatic cooling associated with expansion of the emitting plasma is responsible for the decline of flare. Flaring at a given frequency is produced through the adiabatic expansion of an initially optically thick blob of synchrotron-emitting relativistic electrons. The initial rise of the flux density is produced by the increase in the surface area of blob while it still remains optically thick; the curve turns over once the blob becomes optically thin because of the reduction in the magnetic field, the adiabatic cooling of electrons, and the reduced column density as the blob expands. Such kind of blob ejected from an ADAF is also thought to be a possible explanation for nonthermal flares and recombination X-ray lines in low-luminosity active galactic nuclei and radio-loud quasars (Wang et al. 2000).

Our observed IDVs with different amplitudes and timescales seem consistent with the expanding plasmon model in the context of jet or outflow. The amplitudes and timescales vary with the relativistic particle energy distribution, expanding velocity and size of the blob. To apply the model to the light-curves on 2006 August 12 and 13, we first assumed a power-law spectrum of the relativistic particle energy ($n(E) \propto E^{-p}$). Hornstein et al. (2007) reported a constant spectral index of 0.6 using multi-band IR observations of several flares. Here we adopt a spectral index of 0.6, corresponding to the particle spectral index of 2.2, the energy of the particles was assumed to range from 10 MeV to 3 GeV. The expanding velocity was supposed to be constant. As is stated by Yusef-Zadeh (2008), the relationship between the quiescent and flaring states of Sgr A* is not fully understood. Their results indicate that the quiescent emission at 7- and 13-mm varies on different days. The minimum flux density was 1.5 Jy during our 2006 August observing session, the quiescent flux density, if it does exist, should not be more than this value. We then assume a quiescent flux density of 1.4 Jy, while the flare is produced by the blob. Other parameters were derived by means of the weighted least square method. We adopt exponentially increasing step length for number density during the fitting in order to improve efficiency. The uncertainties of the parameters were assessed by scaling up the 68.3 % confidence region of parameter space, as an increase of χ^2 from χ^2_{min} to $\chi^2_{min} + \chi^2_\nu$ with the reduced chi squares, $\chi^2_\nu = \chi^2_{min}/N_{dof}$, where N_{dof} is the difference between the number of data and the number of fitting parameters (c.f. Shen et al. 2003).

We used two blobs to fit for flare observed on 2006 August 12 and three blobs for those observed on 2006 August 13. Initial magnetic field of 20-50 Gauss were derived from the fit. The electron cooling timescale due to synchrotron loss is (e.g., Marrone et al. 2008)

$$t_{\rm syn} = 38 \left(\frac{\nu}{90}\right)^{-1/2} \left(\frac{B}{10}\right)^{-3/2} [\rm hr]. \quad (1)$$

where the frequency (ν) is in GHz and magnetic field (B) in Gauss. It is about 3.4 hr with a magnetic field of 50 Gauss at 90 GHz, which is comparable to the observed decreasing timescale of 2 hr. Thus the synchrotron cooling of the electrons should not be ignored. We took this into account and re-did the whole fit. The energy loss rate is given by You (1998):

$$(\frac{d\gamma}{dt})_{\rm syn} = -3 \times 10^{-8} \gamma^2 U_{\rm mag}, \quad (2)$$

where $U_{\rm mag} = \frac{B^2}{8\pi}$. With a constant expanding velocity v, the radius of the blob R can be expressed as $R = R_0 + vt$, R_0 is the initial radius of the blob at a specific instant $t_0 = 0$. Substituting B and t with v, R, R_0 and the initial magnetic field B_0, Eq.(2) can be written as

$$(\frac{d\gamma}{dR})_{\rm syn} = \frac{1}{v}(\frac{d\gamma}{dt})_{\rm syn} = -\frac{3 \times 10^{-8} B_0^2 R_0^4}{8\pi v} \gamma^2 R^{-4} = -c_1 \gamma^2 R^{-4} \quad (3)$$

where $c_1 = \frac{3\times10^{-8}B_0^2R_0^4}{8\pi v}$. The energy loss rate due to the adiabatical expanding is

$$(\frac{d\gamma}{dR})_{\rm exp} = -\frac{\gamma}{R}. \tag{4}$$

Thus the total energy loss rate due to both synchrotron cooling and expanding is

$$\frac{d\gamma}{dR} = -\frac{\gamma}{R} - c_1\gamma^2 R^{-4} \tag{5}$$

Eq. (5) is a Bernoulli equation with a solution

$$\gamma = \gamma_0 \left(\frac{R}{R_0}\right)^{-1} \left\{\frac{1}{4}c_1\gamma_0 R_0^{-3}\left[1-\left(\frac{R}{R_0}\right)^{-4}\right]+1\right\}^{-1}. \tag{6}$$

Then the optical depth scales as

$$\tau(\nu,R) = \tau(\nu_0,R_0)\left(\frac{\nu}{\nu_0}\right)^{-(p+4)/2}\left(\frac{R}{R_0}\right)^{-(2p+3)}\left\{\frac{1}{4}c_1\gamma_0 R_0^{-3}\left[1-\left(\frac{R}{R_0}\right)^{-4}\right]+1\right\}^{1-p} \tag{7}$$

and the flux density scales as

$$S(\nu,R) = S(\nu_0,R_0)\left(\frac{\nu}{\nu_0}\right)^{5/2}\left(\frac{R}{R_0}\right)^{3}\frac{1-\exp(-\tau(\nu,R))}{1-\exp(-\tau(\nu_0,R_0))}. \tag{8}$$

where $\tau(\nu_0,R_0)$, $S(\nu_0,R_0)$ are optical depth and flux density for frequency ν_0 at the specific instant t_0. The critical optical depth $\tau_{crit}(R)$, at which the flux density for any particular frequency peaks for radius R, satisfies

$$e^{\tau_{crit}(R)} - \frac{1}{3}(2p+3)\tau_{crit}(R) - C_2(R)\tau_{crit}(R) - 1 = 0 \tag{9}$$

where $C_2(R) = \frac{1}{3}c_1\gamma_0 R_0^{-3}(p-1)\left(\frac{R}{R_0}\right)^{(-4)}\left\{\frac{1}{4}c_1\gamma_0 R_0^{-3}\left[1-\left(\frac{R}{R_0}\right)^{-4}\right]+1\right\}^{-1}$. In the expanding plasmon model of van der Laan (1966), optical depth scales as

$$\tau(\nu,R) = \tau(\nu_0,R_0)\left(\frac{\nu}{\nu_0}\right)^{-(p+4)/2}\left(\frac{R}{R_0}\right)^{-(2p+3)}, \tag{10}$$

and $\tau_{crit}(R)$, the critical optical depth at the maximum of the light curve at any frequency, depending only on p through the equation (Yusef-Zadeh et al. 2006b, 2008)

$$e^{\tau_{crit}(R)} - (2p/3+1)\tau_{crit}(R) - 1 = 0. \tag{11}$$

Comparison between Eq.(7) and (10) indicates that the only difference between these two equations is factor $\left\{\frac{1}{4}c_1\gamma_0 R_0^{-3}\left[1-\left(\frac{R}{R_0}\right)^{-4}\right]+1\right\}^{1-p}$ in the former, which is the result of synchrotron cooling. Similarly, the only difference between Eq.(9) and (11) is factor $C_2(R)$ of $\tau_{crit}(R)$ in the former, which decreases as R^{-4}. The optical depth at which the flux density peaks at t_0 satisfies

$$e^{\tau_{crit}(R_0)} - \frac{1}{3}(2p+3)\tau_{crit}(R_0) - C_2(R_0)\tau_{crit}(R_0) - 1 = 0. \quad (12)$$

For typical values of $p = 2.2$, $B_0 = 20$ Gauss, $\gamma_0 = 20$, $R_0 = 4r_g$ and $v = 0.004c$,

$$C_2(R_0) = \frac{1}{3}c_1\gamma_0 R_0^{-3}(p-1) = \frac{1\times10^{-8}B_0^2\gamma_0 R_0(p-1)}{8\pi v} = 0.08 \ll \frac{1}{3}(2p+3) = 2.5 \quad (13)$$

which implies that $\tau_{crit}(R_0)$ mainly depends on p. Since $c_1\gamma_0 R_0^{-3}(p-1) \propto B_0^2$, B_0 is the most sensitive parameter for the evolution of flux $S(\nu, R)$. To illustrate this, we choose typical values of $p = 2.2$, $\gamma_0 = 20$, $R_0 = 4r_g$ and $v = 0.004c$ and show the resulting model light curves at 90 GHz while B_0 is 10, 20, 30, 40 and 50 Gauss in Figure 4. Results from expanding plasmon model of van der Laan (1966) are shown in dotted lines, and results from expanding plasmon model with synchrotron cooling are shown in solid lines. The differences between two results are significant above 30 Gauss, implying that the synchrotron cooling of electrons should not be ignored for strong magnetic field.

The best-fit model for the light-curve of 2006 August 12 is plotted as a solid line in Figure 5 left. Two blobs were required to fit the data, which were assumed to appear at 7.0 and 10.3 UT. We attribute the turnover in light curve to the birth of a new blob, so the second blob was assumed to appear before the flux increases. The corresponding initial blob radius $1.8^{+1.6}_{-0.6}r_g$ and $2.6^{+0.4}_{-0.2}r_g$, expanding velocity $4^{+2}_{-1}\times10^{-3}c$ and $2^{+2}_{-1}\times10^{-3}c$, electron number density of $2.56_{-2.52}\times10^7\mathrm{cm}^{-3}$ and $5.12^{+5.12}_{-2.56}\times10^7\mathrm{cm}^{-3}$, magnetic field of 19^{+30}_{-5} and 7^{+4}_{-2} Gauss were derived from the fit. The uncertainty that was failed to be assessed was left blank, if not such a sensitive parameter. The peak flux densities of two blobs are estimated to be 0.26 and 0.59 Jy, respectively. The half-power durations are 1.7 and 5.2 hr, respectively. Blob mass of 2.3×10^{20} g and 1.4×10^{21} g were estimated.

Figure 5 right shows the best-fit model for the light-curve of 2006 August 13. Similarly, three blobs appeared at 6.6, 10.0 and 13.0 UT are required to fit the flare. Initial blob radius $4.2\pm0.2r_g$, $2.8^{+0.4}_{-0.6}r_g$ and $2.3^{+0.8}_{-0.4}r_g$, expanding velocity $5^{+1}_{-2}\times10^{-3}c$, $5^{+3}_{-1}\times10^{-3}c$ and $5\pm2\times10^{-3}c$, electron number density of $1.6^{+4.8}_{-1.2}\times10^6\mathrm{cm}^{-3}$, $2.56^{+7.68}_{-2.24}\times10^7\mathrm{cm}^{-3}$ and $5.12_{-4.48}\times10^7\mathrm{cm}^{-3}$ and magnetic field of 23^{+4}_{-8}, 15^{+25}_{-8} and 13^{+8}_{-6} Gauss were derived from the fit. The peak flux densities of three blobs are 0.67, 0.66 and 0.48 Jy, respectively. The half-power durations are 3.2, 2.8 and 2.4 hr, respectively. Blob mass of 1.8×10^{20} g, 8.5×10^{20} g and

9.4×10^{20} g were estimated based on derived parameters. The mass-loss rate contributed by blob was then calculated to be $9.7 \times 10^{-10} M_{\odot}$ yr^{-1}. This value is lower than the accretion rate range $2 \times 10^{-7} M_{\odot}$ yr^{-1} to $2 \times 10^{-9} M_{\odot}$ yr^{-1} estimated by the rotation measure measurements (Marrone et al. 2007). The derived parameters have been summarized in Table 2.

In principle, the expanding plasmon model can also be used to interpret the 2000 March 7 NMA short millimeter flare reported by Miyazaki et al. (2004). In their observation, the peak flux density at the 140 GHz band is apparently larger than that at the 100 GHz band. The spectral variation suggests that the energy injection to photons occurred in the higher frequency regime first and the emitting frequency was shifted to the millimeter-wavelength regime with time, which is well consistent with the scenario predicted by expanding plasmon model. A time delay of 1.5 hr was observed for NIR and sub-mm flare on 2008 June 3 (Eckart et al. 2008b), which has been explained with a similar model with adiabatically expanding source components. There, the spectral index (0.9 to 1.8), expansion velocity (0.005c) and source size ($\sim$2 r_g) are fairly consistent with the parameters derived here. In order to compare with their modeling results, we calculate the optical depth at sub-mm based on parameters derived here. Take the first blob of 2006 Aug 13 for example, according to Pacholczyk (1970), the optical depth at 90 GHz is calculated to be 8.23 at t_0. The critical optical depth at which the flux density for any particular frequency peaks at t_0, is calculated to be 1.82 based on Eq.(12). According to Eq.(7), the optical depth at 345 GHz is 0.14, which is smaller than the critical value. Therefore, at both NIR and sub-mm wavelengths, the emission is optically thin at the beginning. Since we attribute the turnover in light curve to the emergence of a new blob, so the new blob is assumed to appear right before the observed flux density increases. Extending the model in time might help give time delay between NIR and sub-mm, however, the birth time of blob is difficult to determine. Future simultaneous multi-wavelength observation, especially the correlation between optically thin (such as NIR/X-ray) and 3-mm flaring emission is expected to help improve the model fitting.

5.2. The Hot Spot Model

An orbiting hot spot model has been frequently used to mainly explain the observations of short-term NIR and X-ray variability (Broderick & Loeb 2005, 2006, Meyer et al. 2006a, 2006b, Trippe et al. 2007, Eckart et al. 2006b, 2008a). The hot spot is modeled by an overdensity of non-thermal electrons centred at a certain point of its Keplerian orbit. This situation may arise in the case of magnetic reconnection event similar to the solar flare. Due to the Doppler shift and relativistic beaming the approaching portion of the hot spot orbit appears considerably brighter than the receding portion. This model is successful in

explaining the NIR 17 minutes quasi-periodic oscillation (Genzel et al. 2003). The hot spot model is applied to radio band by including the effects of disk opacity for a typical RIAF model (Broderick & Loeb 2006). In these studies, the hot spot is always close to the innermost stable circular orbit (ISCO), thus the NIR 17 minutes quasi-periodic oscillation can be produced. Since the creation of such a hot spot is still under discussion, it is also possible that such kind of spot may appear somewhere away from the ISCO and thus produce quasi-periodic oscillation with a longer timescale.

In the accretion disk, neighboring annuli of differentially rotating matter experience a viscous shear that transports angular momentum outwards and allows matter to slowly spiral in towards the center of the potential (Merloni 2002). As a result, the gas rotates with a sub-Keplerian angular velocity (Narayan et al. 1997). In the following we assume that the rotation of hot spot is also sub-Keplerian and fit our detected IDV events using a sub-Keplerian rotating hot spot model. To simplify the calculation, the angular velocity is assumed to be 0.4 times of Keplerian angular velocity of a Schwarzschild black hole.

We assumed the values of most physical parameters of the hot spot model the same as those in the expanding plasmon model when starting fitting the hot spot model to light-curves. These include: the energy range of relativistic particles, the particle spectral index and the quiescent flux density. Then we estimated other parameters by means of weighted least square method. The magnetic field was assumed to range from 1 to 100 Gauss. In RIAF model, the electron number density of accretion disk is about 2×10^6 cm^{-3} at a distance $20r_g$ from the central black hole (Yuan et al. 2003). Since the hot spot is modeled by an overdensity of non-thermal electrons, it is safe to assume the electron number density ranges from 4×10^6 to 1×10^8 cm^{-3}. In addition, the accretion disk is assumed to be edge-on to maximize the boosting effect (Huang et al. 2007; 2008). The final result is the combination of the quiescent flux density and flux density of hot spot. The derived parameters are summarized in Table 3.

The hot spot model for the 2006 August 12 flaring is plotted as a solid line in Figure 6 left. The quiescent flux density was assumed to be 1.4 Jy. Two hot spots are needed to fit the data. Radius of $6.5 \pm 0.5r_g$ and $8.0 \pm 0.5r_g$, magnetic intensity of 3^{+2} and 1^{+2} Gauss and electron number density of $4^{+26} \times 10^6$ cm^{-3} and $4^{+26} \times 10^6$ cm^{-3} were derived from the weighted least square fitting. The separation to central black hole is $10 \pm 1r_g$ and $12^{+2}_{-1}r_g$.

The hot spot model for the light-curve of 2006 August 13 is plotted as a solid line in Figure 6 right. The quiescent flux density was 1.4 Jy too. One hot spot is required to fit the data. Radius of $4.1 \pm 0.3r_g$, magnetic intensity of 6^{+2}_{-5} Gauss and electron number density of $6^{+44} \times 10^6$ cm^{-3} were derived. The hot spot is at $11.4^{+0.4}_{-0.2}r_g$ from the central black hole.

The electron cooling timescales due to synchrotron losses are calculated to be greater than 2 days at 90 GHz, much longer than the observed variation timescale, thus the synchrotron energy loss can be ignored in the fitting. Since the synchrotron cooling time is long, the life time of hot spot should mainly depend on the dynamical timescale. Reid et al. (2008) analyzed the limits on the position wander of Sgr A*, ruling out the possibility of hot spots with orbital radius above $15r_g$ that contribute more than 30% of the total 7-mm flux. All the orbital radius listed in Table 3 are smaller than $15r_g$. Hence, the presented hotspot model is not in contradiction with their result.

The discussion above shows that both the expanding plasmon model and the orbiting hot spot model can be used to interpret the detected two IDV events. Given that the former model predicts a time delay in flare emission, while the latter does not, the time delay between different frequencies in flare emission is believed to be critical to distinguish between them (Yusef-zadeh et al. 2006b). Recently, Yusef-zadeh et al. (2008) detected time lags of 20.4±6.8, 30±12 and 20±6 minutes between the flare peaks observed at 13-mm and 7-mm. At shorter wavelength, a possible time delay of 110±17 minutes between X-rays and 850-μm was observed (Marrone et al. 2008). Though these observations seem to support the expanding plasmon model, the hot spot model is still a possible explanation, especially for the observed nearly symmetrical light-curves.

6. SUMMARY

We presented the results of the ATCA flux density monitoring of Sgr A* at 3-mm, with emphasis on the detected two IDV events. Comparison of flux densities in two observing sessions in 2006 indicates that Sgr A* appeared to undergo a high state in June session, and a low state in August session. On 2006 August 12, Sgr A* exhibits a 33% fractional variation in about 2.5 hr. Two peaks with a separation of 4 hr are seen on 2006 August 13 flare which exhibits a maximum variation of 21% within 2 hr.

The short timescales inspire us to consider mechanisms other than synchrotron cooling that may be responsible for the variation. Both the expanding plasmon model and the sub-Keplerian rotating hot spot model were discussed and applied to interpret the observed light curves. Because of a relatively large derived magnetic intensity (and thus a short synchrotron cooling timescale), we incorporated the synchrotron cooling into the original adiabatically expanding plasmon model to model the observed IDV data. The radius of blob was estimated to range from 1 to $5r_g$, the expanding velocity range from $0.001c$ to $0.007c$, the electron number density larger than 1×10^6 cm^{-3} and the magnetic field range from 7 to 30 Gauss. A minimum mass-loss rate of $9.7 \times 10^{-10} M_\odot$ yr^{-1} was deduced based on

these derived parameters. We assume that the rotation of hot spot is sub-Keplerian while applying the hotspot model. It seems that both models can reasonably fit the detected IDV events. Future simultaneous multi-wavelength monitoring is expected to discriminate them and tell us where such kind of IDV events come from.

The Australia Telescope Compact Array is part of the Australia Telescope which is founded by the Commonwealth of Australia for operation as a National Facility managed by the CSIRO.

This work was supported in part by the National Natural Science Foundation of China (grants 10573029, 10625314, 10633010 and 10821302) and the Knowledge Innovation Program of the Chinese Academy of Sciences (Grant No. KJCX2-YW-T03), and sponsored by the Program of Shanghai Subject Chief Scientist (06XD14024) and the National Key Basic Research Development Program of China (No. 2007CB815405).

REFERENCES

Baganoff, F.K., et al. 2001, Nature, 413, 45

Balick, B. & Brown, R.L. 1974, ApJ, 194, 265

Bardeen, J.M., Press, W.H., Teukolsky, S.A. 1972, ApJ, 178, 347

Broderick, A. E. & Loeb, A. 2005, MNRAS, 363, 353

Broderick, A. E. & Loeb, A. 2006, MNRAS, 367, 905

Eckart, A. & Genzel, R. 1996, Nature, 383, 415

Eckart, A., Baganoff, F.K., Morris, M. et al., 2004, A&A, 427, 1

Eckart A., Baganoff, F.K., Schödel, R. et al., 2006a, A&A, 450, 535

Eckart, A., Baganoff, F. K., Schödel, R. et al., 2006b, A&A, 455, 1

Eckart, A., Baganoff, F.K., Zamaninasab, M. et al., 2008a, A&A, 479, 625

Eckart, A., Schödel, R., García-Marín, M. et al., 2008b, A&A, 492, 337

Esin, A.A., McClintock, J.E. & Narayan, R. 1997, ApJ, 489, 865

Eisenhauer, F., Schödel, R., Genzel, R. et al. 2003, ApJ, 597, 121

Falcke, H., Goss W. M., Matsuo H., Teuben P., Zhao J.-H. & Zylka R. 1998, ApJ, 499, 731

Genzel, R., et al. 2003, Nature, 425, 934

Ghez, A.M., Morris, M., Becklin, E.E., Tanner, A., Kremenek, T. 2000, Nature, 4007, 803

Glenn, J., Jewell, P.R., Fourre, R. & Miaja, L. 2003, ApJ, 588, 478

Herrnstein, R.M., Zhao, J.H., Bower, G.C., & Goss, W.M. 2004, AJ, 127, 339

Hornstein, S. D., Matthews, K., Ghez, A. M., Lu, J. R., Morris, M., Becklin, E. E., Rafelski, M., & Baganoff, F. K. 2007, ApJ, 667, 900

Huang, L., Cai, M., Shen, Z. & Yuan, F. 2007, MNRAS, 379, 833

Huang, L., Liu, S., Shen, Z.Q., Cai, M.J., Li, H. & Fryer, C.L. 2008, ApJ, 676, L119

Marrone, D.P., Moran, J.M., Zhao, J.H. & Rao, R. 2007, ApJ, 654, L57

Marrone, D.P., Baganoff, M., Morris, M. et al. 2008, ApJ, 682, 373

Mauerhan, J.C., Morris, M., Walter, F., & Baganoff, F. 2005, ApJ, 623, L25

Miyazaki, A., Tsutsumi, T., & Tsuboi, M.. 2004, ApJ, 611, L97

Merloni, A., 2002, in: Cagnoni I. (ed.), Inflows, Outflows and Reprocessing around Black Holes - Proceedings of the 5th Italian AGN Meeting, p.90 [astro-ph/0210251]

Meyer, L., Schödel, R., Eckart, A. et al 2006a, A&A, 458, 25

Meyer, L., Eckart, A., Schödel, R. et al 2006b, A&A, 460, 15

Narayan, R., Kato, S. & Honma, F. 1997, ApJ, 476, 49

Pacholczyk, A. G. 1970, Radio Astrophysics, Freeman, San Francisco

Reid, M.J., Broderick, A.E., Loeb, A. Honma, M. & Brunthaler, A. 2008, ApJ, 682, 1041

Sault, R.J., Teuben, P.J., & Wright, M.C. H. 1995, in Astronomical Data Analysis Software and Systems IV, eds. R. Shaw, H.E. Payne, & J.J.E. Hayers (ASP Conf. Ser., Vol. 77), p.433

Schödel, R., Ott, T., Genzel, R. et al. 2002, Nature, 419, 694

Shen, Z.Q., Liang, M.C., Lo, K.Y. & Miyoshi, M. 2003, Astron. Nachr., 324(S1), 383

Trippe, S., Paumard, T., Ott T., Gillessen, S., Eisenhauer, F., Martins, F., & Genzel, R. 2007, MNRAS, 375, 764

Tsutsumi, T., Miyazaki, A. & Tsuboi, M. 2002, AAS, 200, 4409

Ulich B.L. 1980, Astrophys. Letters, 21, 21

van der Laan 1966, Nature, 211, 1131

Wang, J.M., Yuan, Y.F., Wu, M. & Kusunose, M. 2000, ApJ, 541, L41

Yuan, F., Quataert, E. & Narayan, R. 2003, ApJ, 598, 301

You, J.H. 1998, Radiation Mechanisms in Astrophysics, 2nd ed., Beijing: Science Press, p.182

Yusef-Zadeh, F., Bushouse, H., Dowell, C.D. et al. 2006a, ApJ, 644, 198

Yusef-Zadeh, F., Roberts, D., Wardle, M., Heinke, C.O., & Bower, G.C. 2006b, ApJ, 650, 189

Yusef-Zadeh, F., Wardle, M., Heinke, C. et al. 2008, ApJ, 682, 361

Zhao, J.H., Herrnstein, R.M., Bower, G.C., Goss, W.M. & Liu, S.M. 2004, ApJ, 603, L85

This preprint was prepared with the AAS LaTeX macros v5.0.

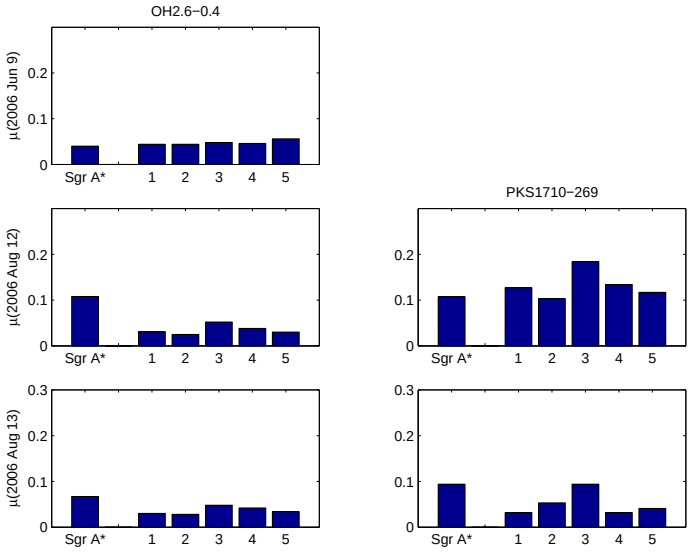

Fig. 1.— Modulation index of flux density of Sgr A*, and gain corrections of five antennas (labeled 1, 2, 3, 4 and 5). They are derived from calibrators OH2.6-0.4 and PKS 1710-269 (from left to right) for three observations on 2006 June 9, August 12 and 13 (from top to bottom). Many data obtained from antenna 3 in August session were shadowed and have been flagged, so the uncertainty of this antenna is big compared with other antennas. During observation in 2006 August, the 3-mm flux density of PKS 1710-269 was around 0.5 Jy, only one fiftieth of that of OH2.6-0.4, therefore the modulation index of gain corrections derived from this source are particularly high.

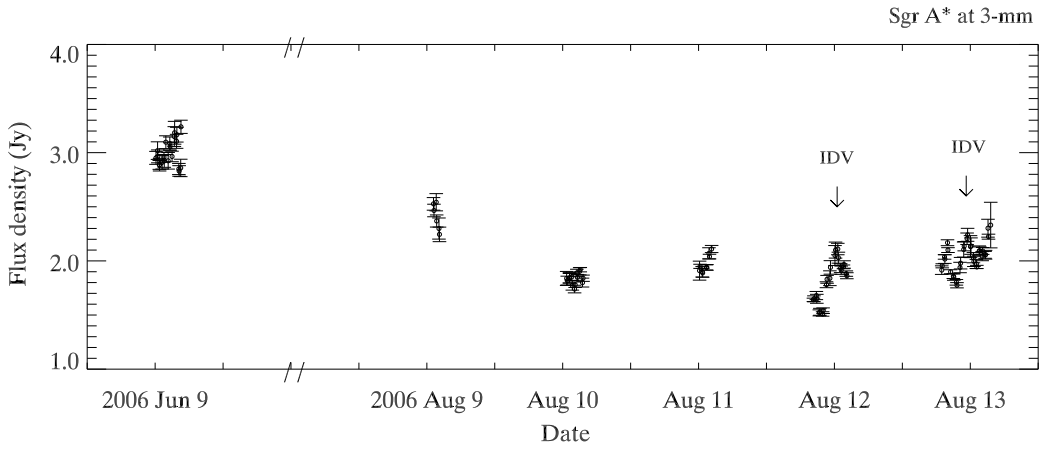

Fig. 2.— ATCA 3-mm light-curves of Sgr A* in 2006. Two detected IDV events are indicated (arrows).

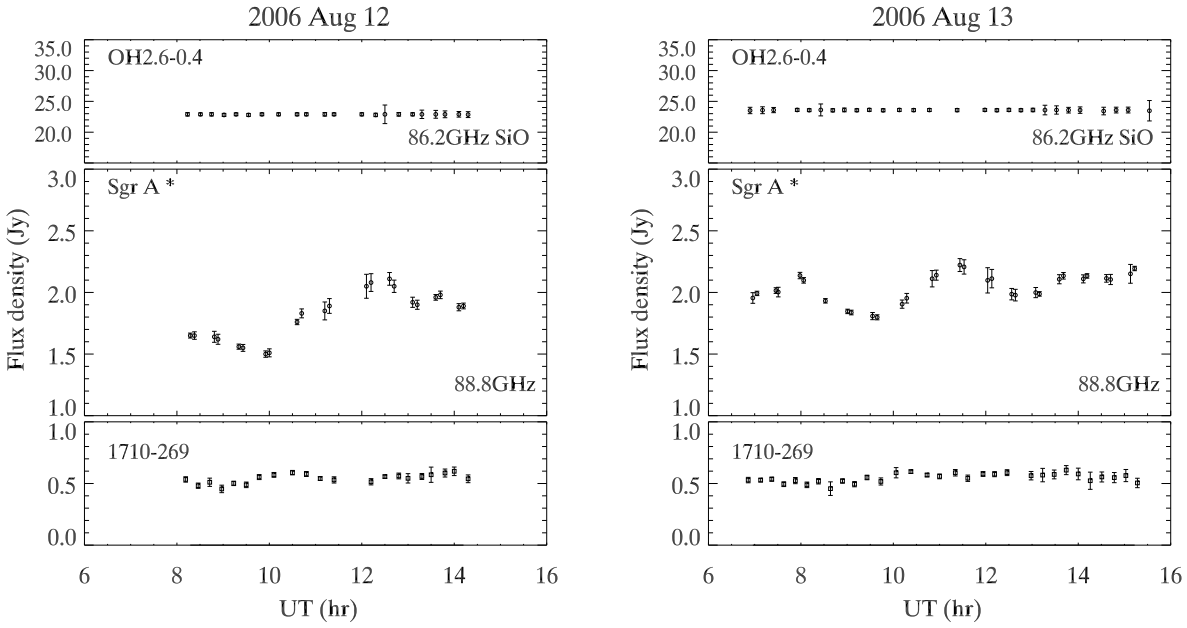

Fig. 3.— ATCA 3-mm light-curves on 2006 August 12 (Left) and 13 (Right) of Sgr A* (middle panel), secondary calibrators OH 2.6-0.4 (top panel) and PKS 1710-269 (bottom panel).

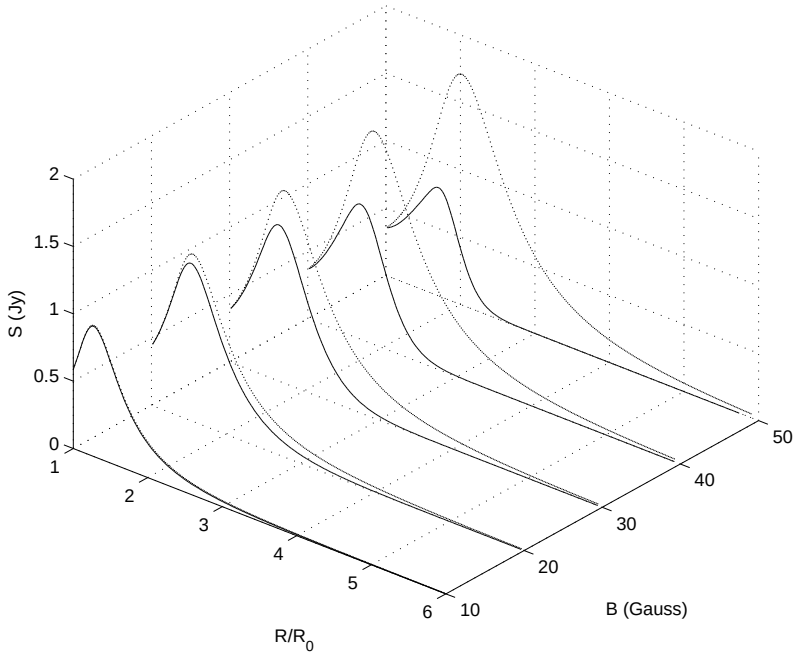

Fig. 4.— Two kind of theoretical model light curves as a function of expanding blob radius at 90 GHz with different B_0. Results from expanding plasmon model of van der Laan (1966) are shown in dotted lines, and results from expanding plasmon model with synchrotron cooling are shown in solid lines.

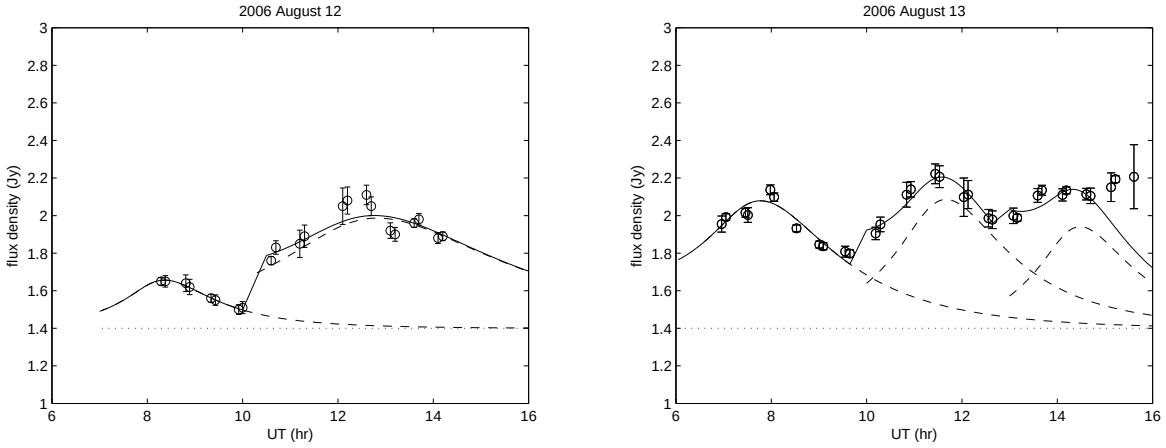

Fig. 5.— The solid line represents the expanding plasmon model fitting to the observed 3-mm light-curves on 2006 August 12 (left) and 13 (right) with synchrotron radiation cooling taken into account. An assumed quiescent flux density of 1.4 Jy is indicated by the straight dotted line. The blobs used to fit the data are indicated by dashed curves.

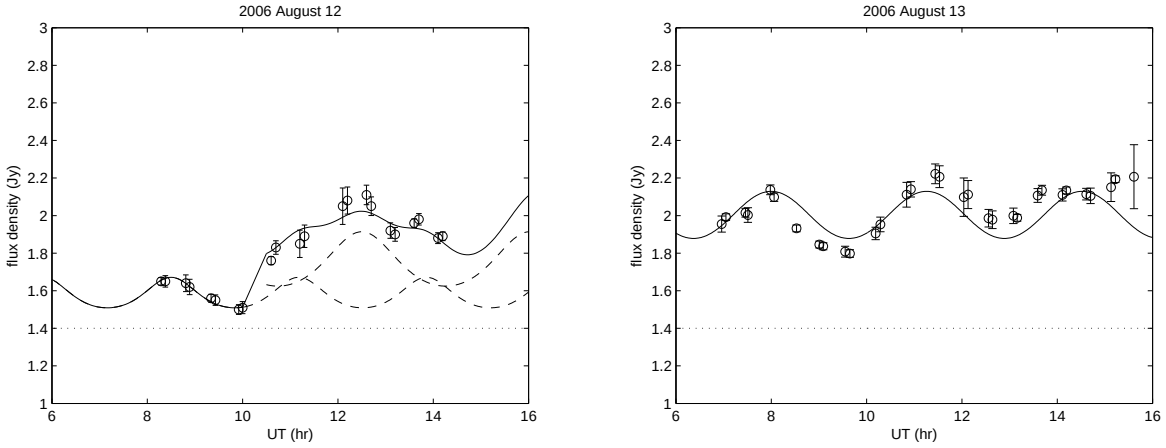

Fig. 6.— The light-curves produced by the sub-Keplerian orbiting hot spot model on 2006 August 12 (left) and 13 (right). An assumed quiescent flux density of 1.4 Jy is indicated by the straight dotted line. Two hot spots used to fit the data on August 12 (left) are indicated by dashed curves.

Table 1: ATCA Observations of Sgr A* in 2006. Length is duration of the observation. IF1&IF2 are intermediate frequencies for the lower and upper sidebands, respectively, with the corresponding bandwidth of BW1&BW2. Range of baselines are indicated by uv range. Beam is the ATCA synthesized beam.

Date	Length (hr)	IF1&IF2 (GHz)	BW1&BW2 (MHz)	uv range (kλ)	Beam
2005 Oct 18	10	93.504&95.552	128&128	13-61	$2.''9 \times 1.''7$
2006 June 9	6	86.243&88.896	16&128	20-430	$2.''1 \times 0.''3$
2006 Aug 9	1				
2006 Aug 10	4				
2006 Aug 11	2	86.243&88.896	16&128	3-570	$1.''3 \times 0.''2$
2006 Aug 12	7				
2006 Aug 13	9				

Table 2: Parameters of the expanding plasmon model. We took into account the synchrotron cooling of electrons while applying the adiabatically expanding plasmon model to the light-curves. Here, t_0 is the time at which the blob was assumed to be generated, R_0 is the initial radius, v is the expanding velocity, N_0 is the initial electron number density, B_0 is the initial magnetic field strength, $S_{\rm p}$ is the peak flux density of the blob, and χ^2_ν is the reduced chi squares.

Date	t_0(hr)	$R_0(r_g)$	v (10^{-3}c)	N_0 (cm^{-3})	B_0(Gauss)	$S_{\rm p}$(mJy)	χ^2_ν
2006 Aug 12	7.0	$1.8^{+1.6}_{-0.6}$	4^{+2}_{-1}	$2.56_{-2.52} \times 10^7$	19^{+30}_{-5}	0.26	1.64
	10.5	$2.6^{+0.4}_{-0.2}$	2^{+2}_{-1}	$5.12^{+5.12}_{-2.56} \times 10^7$	7^{+4}_{-2}	0.59	
2006 Aug 13	6.6	4.2 ± 0.2	5^{+1}_{-2}	$1.6^{+4.8}_{-1.2} \times 10^6$	23^{+4}_{-8}	0.67	3.60
	10.0	$2.8^{+0.4}_{-0.6}$	5^{+3}_{-1}	$2.56^{+7.68}_{-2.24} \times 10^7$	15^{+25}_{-8}	0.66	
	13.0	$2.3^{+0.8}_{-0.4}$	5 ± 2	$5.12_{-4.48} \times 10^7$	13^{+8}_{-6}	0.48	

Table 3: Parameters of the sub-Keplerian orbiting hot spot model. R is the radius of hot spot, N_e is the electron number density, B is the magnetic field strength, D is the distance between hot spot and the central black hole, and χ^2_ν is the reduced chi squares.

Date	R (r_g)	N_e (cm^{-3})	B (Gauss)	D (r_g)	χ^2_ν
2006 Aug 12	6.5 ± 0.5	$4^{+26} \times 10^6$	3^{+2}	10 ± 1	1.04
	8.0 ± 0.5	$4^{+26} \times 10^6$	1^{+2}	12^{+2}_{-1}	
2006 Aug 13	4.1 ± 0.3	$6^{+44} \times 10^6$	6^{+2}_{-5}	$11.4^{+0.4}_{-0.2}$	12.32